Simultaneous In-Process Control of Heat-Affected Zone and Cooling Rate during Arc Welding

A model is developed for independently regulating the time-temperature relationship of the HAZ and the centerline cooling rate

BY C. C. DOUMANIDIS AND D. E. HARDT

ABSTRACT. The problem of process control in welding involves not only regulation of weld bead geometry, but also thermally induced changes such as distortion, residual stresses and metallurgical transformations near the weld. This paper addresses the last of these, and poses it as a feedback control problem. The objective is transformed to one of controlling the surface temperature field in-process, and using temperature feedback to implement such a scheme. A control model of the process is presented, and a parameter adaptive controller is designed to ensure consistent control system performance. A series of numerical simulations and experiments using GMA welding is presented that confirms the model and illustrates the desired properties of the controller. With this system, the heat-affected zone and cooling rate (through their correlates in surface temperature-time relationships) can be regulated independent of each other, and gross disturbances to the temperature field rejected totally in the steady-state. In addition, dynamic performance of the control system is illustrated, and the limits imposed by current hardware are discussed.

Introduction

Recent interest in real-time control of welding processes has concentrated primarily on control of geometric attributes of the weld (Refs. 1, 2). While geometry is indeed a primary determinant of weld quality, a complete welding control system must also include the thermal effects of distortion, residual stress and metallurgical transformation close to the weld. In addition, a welding control system must be able to simultaneously regulate all of the weld variables of interest, taking into account the highly coupled nature of the typical process inputs and outputs.

This paper addresses the problem of in-process control of several metallurgical transformation mechanisms. The importance of such control can be realized by considering weld joints with acceptable bead geometry and negligible residual stresses and distortion, but with highly imperfect final microstructure, particularly in cases involving extensive solidification defects, sensitization zones or martensitic weld beads (Refs. 3–6). Such weld imperfections can be attacked in-process by modulating either the filler material composition or the thermal history of the process. Since the former is impractical to manipulate in-process, modulation of the heat input will be adopted herein to effect the control authority.

The "open-loop" block diagram of the process in Fig. 1A shows quantities reflecting final microstructure and material properties as system outputs, however, they are typically not measurable in-process. But, since these properties are usually well-behaved functions of temperature field characteristics (Refs. 7, 8), it is possible to measure the latter for feedback and still use open-loop control of the final microstructure and the resulting material properties. This is not overly restrictive, since most process uncertainties and external disturbances appear in the thermal process, inside the proposed control loop—Fig. 1B.

To develop the control system, the first task is to define a set of measurable outputs that will adequately describe the microstructural and material characteristics. These then must be controlled to reference or command values using suitable welding inputs. The latter are selected so as to insure efficient and decoupled (independent) modulation of the chosen outputs.

KEY WORDS

In-Process Control
Arc Welding
Heat-Affected Zone
HAZ Control
Cooling Rate Control
Simultaneous Control
Adaptive Control
GMA Welding Model
Metallurgical Transformation
Heat Input Modulation

Selection of the Welding Outputs

The definition of the welding outputs (those that can be measured and controlled) is based on the relationship between thermal history and resulting metallurgy, which was extensively reviewed in (Refs. 7 and 8) for various commonly welded materials, ranging from plain carbon steels to titanium alloys. This review identified classes of common metallurgical mechanisms activated in these materials during welding, as well as common potential problems affecting the final microstructure and mechanical properties. From this review, the following outputs are selected:

1) The weld nugget cross-section area (NS), defined by the solidus isotherm T_m. This is adopted as a collective measure of the effect of solidification faults, such as porosity, inclusions, incomplete fusion, shrinkage microcracks, columnar structure, uneven grain size, microsegregation and nucleation of undesirable phases in the weld bead (Ref. 3). It can also be employed to determine the dilution of the base metal with additional material, when

C. C. DOUMANIDIS is a Research Associate and D. E. HARDT is Director and Associate Professor of Mechanical Engineering, MIT, Cambridge, Mass.

Paper presented at the 70th Annual AWS Meeting, held April 2–7, 1989, in Washington, D. C.

a consumable electrode or filler metal of different composition is used, as in welding of mild steel with an austenitic electrode, where the martensitic region of the Maurer diagram must be avoided (Ref. 4).

2) The heat-affected zone width (HZ), defined by an enveloping isotherm T_h. This may indicate the extent of weak material zones, such as the recovery, recrystallization and grain growth areas, or the width of the zone in which some undesirable, thermodynamically favored phase is formed, such as the sensitization zone in stainless steels (intergranular nucleation of Cr_4C, (Ref. 5), or the overaging zone of precipitation-hardened aluminum alloys (coalescence and growth of θ-phase particles, (Ref. 6)).

3) The centerline cooling rate (CR), defined at the location with a critical temperature T_c. The centerline (maximum) cooling rate may decide the crystallization of undesirable, kinetically favored phases, such as the martensite of high-carbon steels, or supply a measure of the cracking tendency of the weldment, caused by thermal stresses or various kinds of structural embrittlement, especially in high-alloyed steels and hot short materials (Refs. 7, 8).

These outputs are illustrated in Fig. 2. Note that NS is defined for one of the symmetric plates only, HZ is measured from the center of the weld bead and CR is dynamically defined in the Lagrangian sense at the material point x_c. All three can be evaluated in terms of time varying isotherm locations, and the difficulty of measuring these will be addressed later in the context of control system design.

Selection of the Welding Inputs

Since the goal of this work is to develop a closed-loop control scheme, what is sought here is a causal or control model of the process. Outputs NS, HZ and CR must be paired with a like number of input variables that exert a substantial and independent influence on these outputs (otherwise referred to as sensitivity and decoupledness). Candidate input variables were explored by a comprehensive literature review of the temperature field models (Ref. 9), typically classified as: analytical models, *e.g.*, (Refs. 10–12); empirical models, *e.g.*, (Refs. 13–15); and numerical models, *e.g.* (Refs. 16–19).

None of the models reviewed detailed the input-output dynamics in a manner sufficient for in-process control purposes, and the development of such a model is a major part of this work (see Doumanidis and Hardt for details) (Ref. 20). However, in identifying candidate inputs, the classical thermal conduction model (Refs. 10,11) provides a useful tool for examining sensitivity and decoupledness. Under the assumptions of an infinite plate geometry; homogeneous, isotropic, temperature-invariant material properties with no phase transformations; and conductive heat flow with no surface losses, the steady-state temperature field developed by either a line or point moving source can be solved for the maximum width of the T_m and T_h isotherms and centerline cooling rate at T_c. This yields the following expressions of the welding outputs as functions of the heat input Q, torch velocity v and preheat temperature T_o:

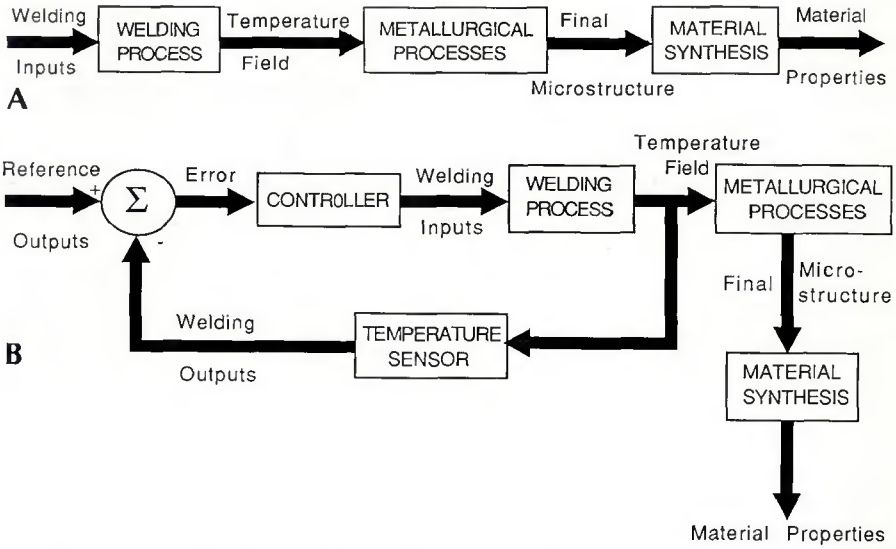

Fig. 1—Schematic causality of the welding process. A—Open-loop control; and B—closed-loop control.

$$NS = c_1\left(\frac{Q}{V^g}\right)^{n_a}\left(\frac{1}{T_m - T_o}\right)^{n_a} \quad (1a)$$

$$HZ = c_2\left(\frac{Q}{v^f}\right)^{1/n_b}\left[\left(\frac{1}{T_h - T_o}\right)^{1/n_b} - \left(\frac{1}{T_m - T_o}\right)^{1/n_b}\right] \quad (1b)$$

$$CR = c_3\left(\frac{Q}{V^f}\right)^{-n_c}\left(\frac{1}{T_c - T_o}\right)^{-(n_c+1)} \quad (1c)$$

where T_m = melting temperature, T_h = HAZ critical temperature, T_c = cooling rate critical temperature, $f = n_b - (n_b - n_2)/(n_3 - n_2) = 1$, $g = 2/3$ a and $n_2 = 0.96$, $n_3 = 1.7$ (obtained from Ref. 16). The coefficients c_1, c_2, c_3 and the exponents n_a, n_b, n_c depend on the geometry and material of the plates as well as on the specific environmental and process conditions, and were evaluated in Ref. 9 on the basis of conduction theory.

Because of the differing exponents for all three outputs, the heat input Q and torch velocity v will exert different influences on all three outputs. Thus, they are clearly suitable as welding inputs. The candidate for the third input is the preheat temperature T_o. However, the use of T_o as a direct control input (implemented, for example by a leading preheat torch) would cause problems of nonuniformity and time delay. On the other hand, since the exponent of the term $1/(T_c - T_o)$ in the expression for CR (Equation 1c) is different from that of the Q/v term, it is possible to exploit this selective dependence by employing a second torch trailing a fixed distance x behind the main torch—Fig. 3. In this way, the main torch has a preheating effect on the CR. Accordingly, the heat input of the primary torch Q_1, the heat input of the secondary torch Q_2, and their common travel speed v are adopted as the inputs to the welding process.

As illustrated in Fig. 4, the heat input of the secondary torch Q_2 can be modulated

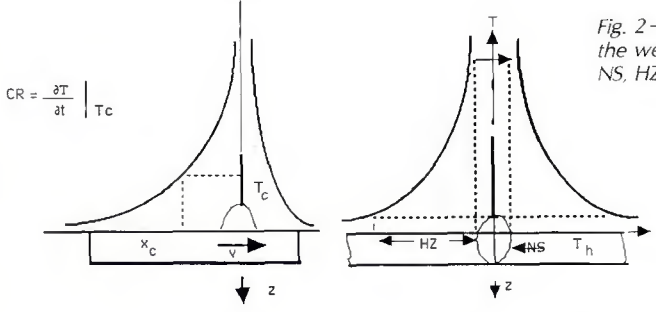

Fig. 2—Definition of the welding outputs NS, HZ and CR.

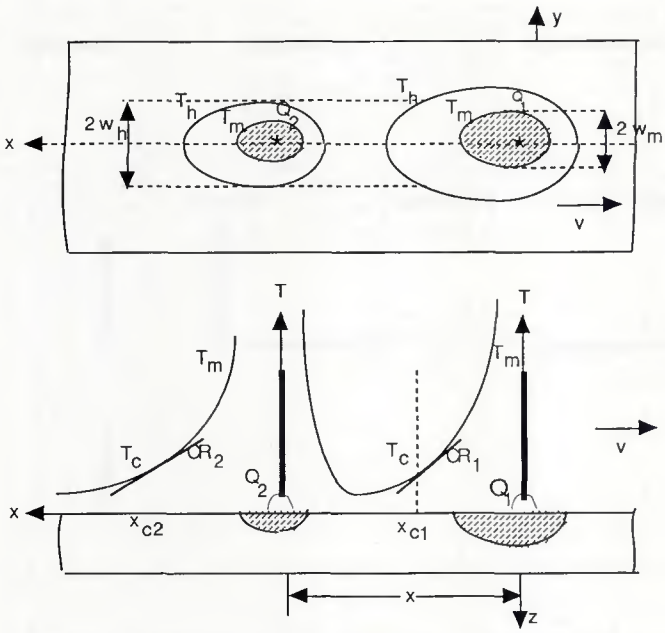

Fig. 3 – The double welding gun configuration and temperature field.

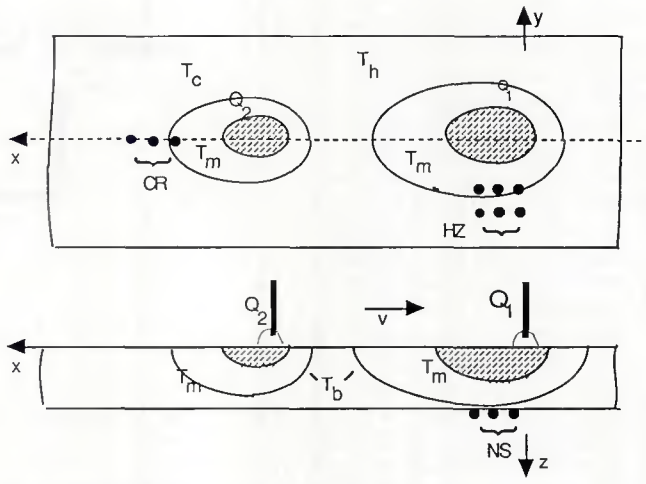

Fig. 4 – The temperature measurement system.

in a restricted range, insuring that the bead cross-section and the heat-affected zone generated by the secondary torch do not exceed the magnitudes of those of the primary torch, and thus NS and HZ are exclusively determined by the main torch characteristics (Q_1, v). Within this range, Q_2 exerts a virtually decoupled effect on CR, without affecting NS or HZ, because of the selectivity of the preheating effect on the cooling rate. Thus, the use of a secondary torch can be thought of as an in-process implementation of a postheating cycle, or as reshaping of the temperature field by using an additional source, affecting the cooling rate only. To determine this control range of CR by the secondary torch, an optimization problem was solved in Ref. 9, on the basis of the steady-state conduction model for both a line and point source, assuming $T_h = T_c$. This determined the optimum values of the secondary torch distance x and heat input Q_2 for which the absolute value of the cooling rate CR is minimized, without affecting the other outputs NS and HZ. The maximum obtainable reduction of CR was found to be 25–38.5% for the double torch configuration. If a broader control range is desired for CR, a multiple torch configuration can be employed. Again, an optimization problem for N distinct torches, arranged along the centerline, determined that CR can be reduced by 50–100% as $N \rightarrow \infty$, without affecting NS and HZ. Of course, a continuous heat distribution along the centerline is another possibility to be examined.

Steady-State Control

From the introduction it is clear that each desirable welding situation will be associated with a desirable set of specifications for NS, HZ and CR. The multivariable, adaptive, feedback control system illustrated in Fig. 5 is intended for the regulation of the welding outputs $\underline{Y}$ (through modulation of the inputs $\underline{U}$) to such reference values $\underline{Y}_d = [NS_d\ HZ_d\ CR_d]^T$. The temperature measurements are used not only for the evaluation of the welding outputs, but also for the identification of the model parameters that tune the controller. Thus, based on the steady-state model above, each sampling period T (*i.e.*, iteration) of the control system shown in Fig. 5, would consist of the following steps:

1) Wait until the welding outputs reach steady state.

2) Verify the values of the welding inputs $\underline{U}(t\text{-}T)$.

3) Evaluate the current welding outputs $\underline{Y}(t)$ using the spot temperature measurements.

4) Identify the model parameter estimates $\underline{\Theta}(t)$ from $\underline{Y}(t) = f(\underline{\Theta}(t), \underline{U}(t\text{-}T))$, using the spot temperature measurements.

5) Determine the necessary inputs $\underline{U}(t)$ to obtain the desired outputs $\underline{Y}_d$ by solving $\underline{Y}_d = f(\underline{\Theta}(t), \underline{U}(t))$.

6) Apply $\underline{U}(t)$ and repeat the procedure from Step 1 for the next iteration.

However, the control system design must take into account the dynamics of the thermal processes, otherwise severe stability and speed limitations will be imposed. An analytical approach would employ the transient conduction model, based on the integration of the appropriate Green's function (Refs. 9,11). However, the derivation of dynamic welding input-output dependencies from this solution was discouraged by its impracticality and limited scope of application owing to the Rosenthal assumptions. Accordingly, a nonlinear, dynamic simulation of

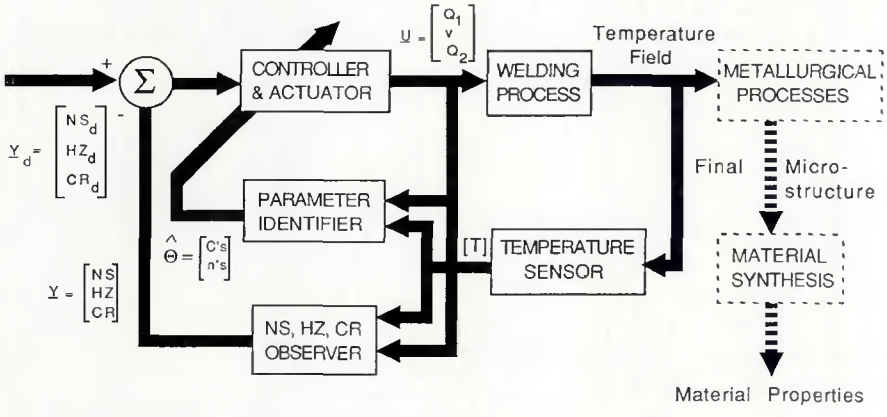

Fig. 5 – The multivariable adaptive closed-loop control scheme.

the relevant heat transfer in the weldment was developed based on a finite difference formulation and is described below in detail. However, it is first necessary to consider the practical aspects of real-time measurement for control.

First of all, we must at this time abandon the use of NS as a welding output since the means to measure NS does not yet exist. However, for the measurement of HZ and CR, an infrared (IR) camera can be used. The ability of scanned infrared cameras to perform rapid line scan thermal measurements also motivates the redefinition of the remaining two welding outputs (Fig. 6) in the following way. Assume that the scan lines of such a camera can be instantaneously aligned with either axis of travel. Now, instead of specifying the isotherm temperature T_h and controlling its width to w_h, it is possible to specify a parallel sideline, at distance $w_p = w_h$ from the centerline, and regulate the peak temperature on it to $T_p = T_h$. This peak temperature T_p requires a single sensor line scan along the sideline per sampling period and is more nearly linear than HZ, because of the smaller spatial variation of its occurrence location (x_p, w_p).

The cooling rate ($CR = \partial T/\partial t/_{T_c}$), because of the time differentiation involved, requires at least two successive line temperature scans along the centerline per sampling period. However, it can be integrated over the time T instead, and yield the temperature drop T_d of the centerline point x_d, which was at critical temperature T_c at the previous sampling instant:

$$T_d(t) = \int_{t-T}^{t} \frac{\partial T}{\partial x}_{x_c} d\tau = |T(t) - T(t-T)|_{x_c} \quad (2)$$

The evaluation of T_d requires a single sensor line scan along the centerline per sampling period, and it is less noisy than CR as a welding output.

In selecting the necessary two welding inputs, the welding gun velocity v is eliminated because of its slow nonlinear influence on the welding outputs (see Equation 3). Implementing primary and secondary heat inputs Q_1 and Q_2 is best done using an autogenous torch for the trailing source. However, for the ensuing experiments, a time-shared single torch technique was employed. This is done by performing a cycling motion along the centerline with constant period T_t, which imitates the action of two separate welding guns at fixed separation distance x, moving at a constant net common speed $v = 1/T_t$, as shown in Fig. 7. This illustrates the geometry, kinematics and power distribution of the i-th torch cycle steps:

The sectional velocities v_1 and v_2 (selected so that T_t is constant) and arc power Q (held constant during each cycle of the welding gun, which are used for the modulation of the welding inputs Q_1 and

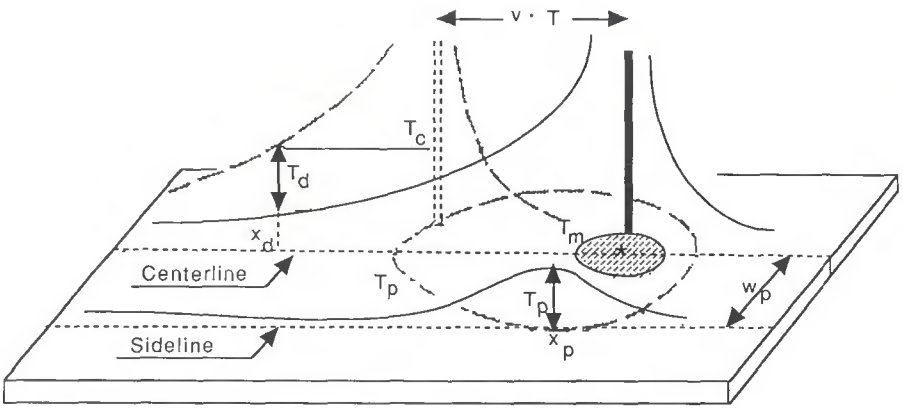

Fig. 6 – Definitions of the welding outputs T_p and T_d.

Q_2 of the resulting continuous heat distribution along the centerline, are determined as follows:

$$v_1 = (1 + Q_2/Q_1)1/T_t$$
$$v_2 = (1 + Q_1/Q_2)1/T_t \quad (3)$$
$$Q = (Q_1 + Q_2)T_t/(T_t - t_{01} - t_{02})$$

The key to such time sharing is that the characteristic time of the cycle (T_t) must be at least half that of the characteristic time of the control system (cycle time T). Thus the system considered below for modeling and control experiments comprises a single time-shared welding gun and two outputs: T_p and T_d.

Process Modeling

In order to model the dynamic dependencies between the two welding outputs (T_p, T_d) and inputs (Q_1, Q_2) of the 2 × 2 welding configuration, and rather than resorting to the idealized analytic transient expression of Equation 3, a numerical simulation of the temperature field for the multi-gun configuration was developed (Ref. 40). The computational simulation program integrates the unsteady conduction equation (Fourier), in discrete time steps Δt and space elements Δs, by employing an explicit Euler finite differ-

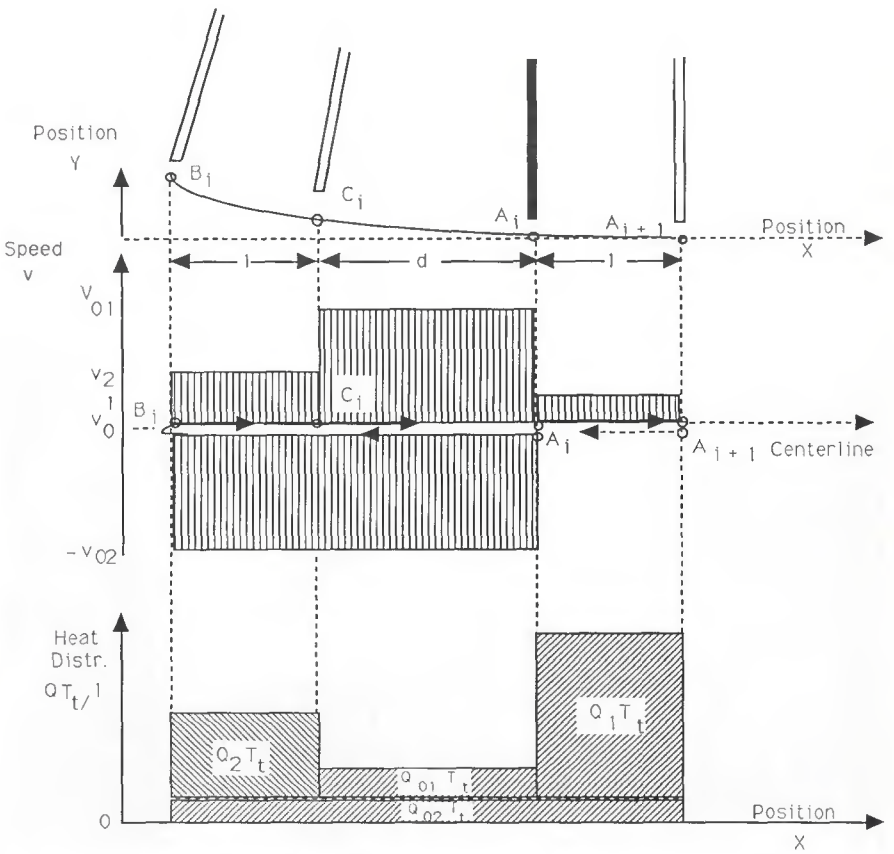

Fig. 7 – Welding gun position, speed and heat input during a gun cycle.

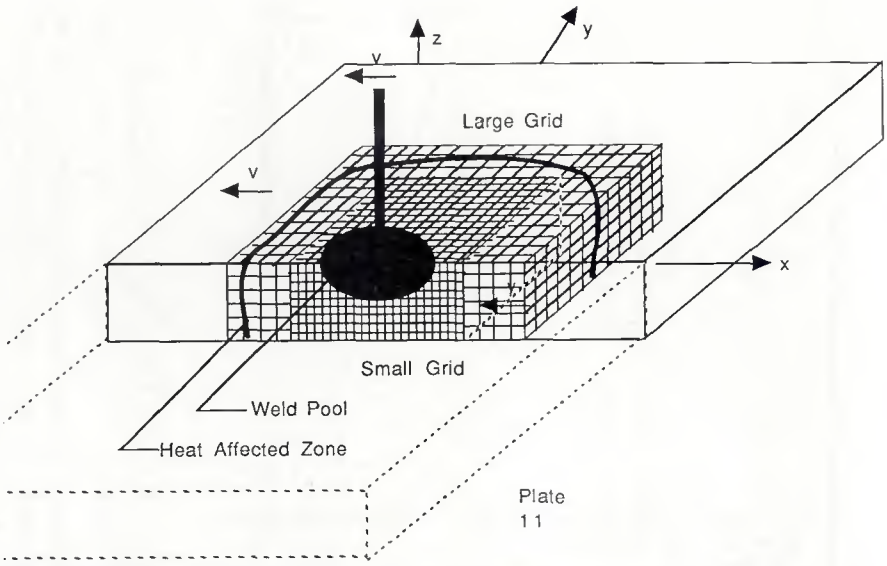

Fig. 8—Geometrical arrangement of the numerical simulation for fusion welding process.

ence formulation:

$$\frac{\partial T}{\partial t} = \nabla^2 T \rightarrow T(t + \Delta t) = T(t) + \frac{\alpha \Delta t}{\Delta s^2}\left[\sum_{i=1}^{6} T_i - 6T(t)\right] \quad (4)$$

where T(t) is the temperature of a location time t and $T_i(t)$ the temperatures of its neighboring points at distance θs in the three dimensions. Alternate forms of Equation 4 in the presence of conductive, convective and radiative boundary conditions along with the program documentation are given in Ref. 20. The main features include the use of fine and coarse node grids (enveloping the T_m and T_h isotherms therms respectively, as shown in Fig. 8), the ability to handle an arbitrary number of welding guns, each with a unique heat input distribution, and the provision for temperature-dependent material properties. While the method considers only conduction in the weldment, the convective heat transfer in the weld pool is accounted for by directional equivalent conduction factors, determined experimentally and reported in the literature (Refs. 22–25). The time histories of heat inputs and speed of the welding guns are arbitrary, to enable simulation of realistic control action.

The numerical model requires experimental calibration of a number of parameters, namely the arc efficiencies of the welding guns, the heat input distribution radii and the equivalent conduction factors in the melt. The rest of the necessary calorimetric data for the heat transfer to the environment, as well as the material thermal properties and their temperature dependence, are taken from the literature (Refs. 17,34,22–25).

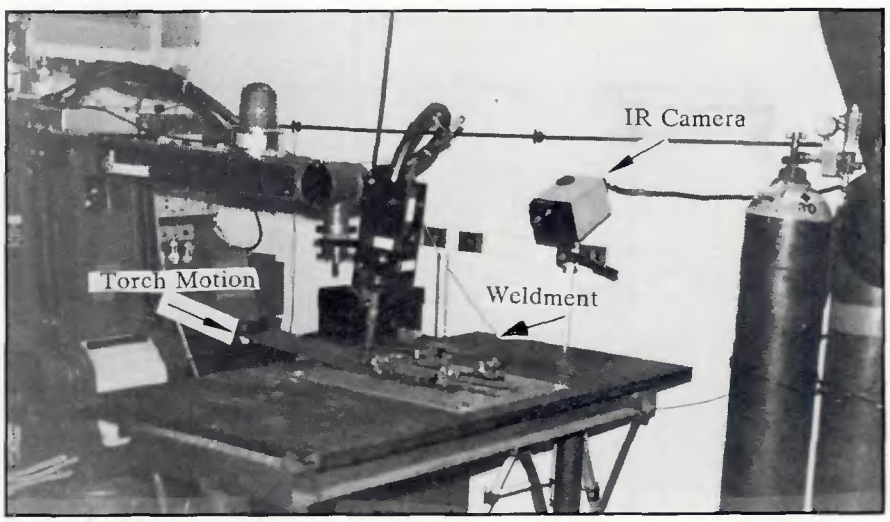

Fig. 9—Experimental implementation of the thermal control system.

Experiments and Model Calibration

The calibration (as well as all subsequent welding experiments) comprised GMA welding of thin mild steel plates, ⅛-in. (3.2 mm) thick. Argon-2% oxygen shielding gas was used, flowing at 50 ft^3 (106 L/min). The welding wire was ER70S-6, 0.035-in. diameter. Nominal open-circuit voltage was 30 V and the wire feed rate was 400 in./min. All experiments were executed with a travel speed of 12 in./s (305 mm/s). All welding parameters were controlled by an Automatix AI-50 welding robot. The gun cycling necessary for time-sharing the heat input was implemented using the fast joint-interpolated motion of a single robot joint for the three first segments, shown exaggerated in Fig. 7. The arc power Q was manipulated through the welding voltage V, so that its product with the current I (nearly constant owing to a constant wire feed) provides the necessary Q = VI.

The on-line thermal measurements consist of scanning the time-dependent temperature field on the top surface of the plates, using an infrared radiation camera system (Ref. 26), sensitive in the range of 8–14μm (HgCdTe detector, $1N_2$ cooled). The mechanical scanner is stationary relative to the welded pieces (Fig. 9), with its horizontal axis parallel to the weld centerline at a distance of 0.8 m and viewing angle of 30 deg relative to the plane of welding. The resulting field of view is 300 × 40 mm, with a spatial resolution of 1.2 × 0.2 mm, and the dynamic temperature range varies between 400–1400 K, with a temperature resolution of 1 K. The infrared pyrometry images are stored using standard video format and analyzed offline, using a thermal image processor (Ref. 27), to determine isotherms and thermal profiles. The temperature distribution of the centerline is used to determine T_d, defined at the austenitization temperature $T_c = T_{A1} = 996$ K for a sampling period T = 2.4 s, and that of the sideline is used to determine T_p at distance $w_p = 10.5$ mm, corresponding to the width of an assumed recrystallization zone—Fig. 10.

The experimental calibration of the numerical simulation parameters is performed so that the computed responses fit the experimental data during an initial transition to the nominal conditions—Fig. 11. These are a set of input values: $Q_1^* = 2500$ W, and $Q_2^* = 250$ W that produce welding outputs corresponding to $T_p^* = 824$ K and $T_d^* = -96.5$ K, which are approximately in the middle of the specified or desirable range. Since T_d is not defined during the first T = 2.4 s, an upper bound of $|T_d| = (T_c - T_o)$ is used instead in Fig. 11. The calibration yields an arc efficiency $\eta = 0.87$, heat distribution width $\sigma = 1.7$ mm, equivalent conduction factor c = 3.6, and IR emissivity $\epsilon = 0.69$, deter-

mined by matching the nominal top surface width of the solidus isotherm T_m = 1738 K to the actual weld bead width.

Development of Process Transfer Functions

Starting at these nominal conditions, the process dynamics are identified by obtaining the responses of the welding outputs T_p and T_d to both positive and negative steps of each welding input Q_1 and Q_2 separately. This was done both by simulation and by experiment, with example results shown in Figs. 12 and 13.

Note that while each step exhibits different steady-state gains and response times, each transient can be approximated by delayed, critically damped, second order behavior (shown by the dot-dashed line), described by the differential equation:

$$\ddot{y}(t) + 2\omega\dot{y}(t) + \omega^2 y(t) = K\,\omega^2 u(t - d) \quad (5)$$

where ω is the natural frequency of the equivalent second order system, K is the steady-state gain, y(t) is $T_p - T_p^*$ or $T_d - T_d^*$, u(t) is $Q_1 - Q_1^*$ or $Q_2 - Q_2^*$, and d is an input delay time. Such critically damped systems can often be approximated by an first order system such as:

$$\tau_{eq}\dot{y}(t) + y(t) = K\,u(t - d) \quad (6)$$

which is intended to simplify the control system design. The differential equation parameters K, τ, d, identified by fitting the responses of the linearized model to the previous experimental data, are collected in Table 1, and their different estimates for positive and negative input steps of the same size demonstrate the nonlinearity of the original model and the consequent need for in-process parameter adaptation.

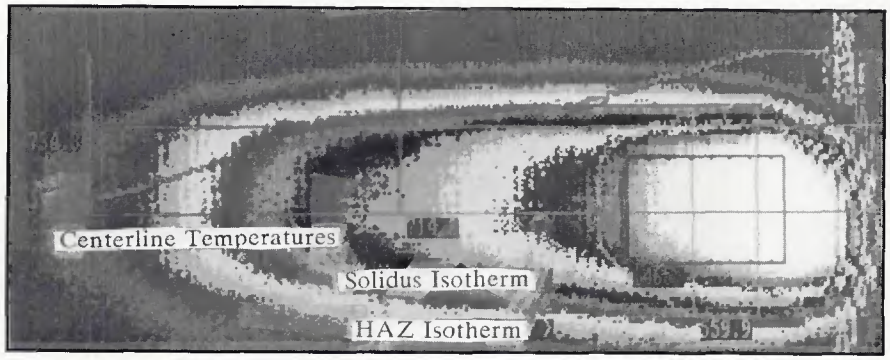

Fig. 10—Top surface temperature field at the nominal conditions.

Thermal Control System

The nonstationary characteristic of the dynamic process model imposes several design requirements on the control strategy. It must deal with the multiple input-output nature of the system, while providing an in-process parameter adaptation capability to track the variable time constants, gains and delay terms. Among various techniques offered by control theory, a discrete-time, multivariable, adaptive control algorithm (Ref. 28) will be adopted for the thermal control system as best suited to the above requirements. This "dead beat" controller follows the same general philosophy as the steady-state strategy before, the main difference being that controller parameters are estimated by a recursive adaptation law:

$$\hat{\Theta}(t) = \hat{\Theta}(t-T) + \gamma(t)[\hat{\Theta}(t-T)\Phi^T(t-D)]\,\Phi^T(t-D) \quad (7)$$

where $\underline{\Theta}(t)$ consists of the dynamic model parameters (which include the Ts and Ks from Equation 6) and $\Phi(t)$ is a dynamic register vector comprising outputs $\underline{y}(t) = [T_p\ T_d]$ and the inputs $\underline{u}(t) = [Q_1 Q_2]$ together with previous input-output history. The necessary input values $\underline{u}(t)$ to obtain tracking of the reference outputs $\underline{y}_d(t) = [T_p\ T_d]_d$ after a delay d are obtained by solving the control law:

$$\underline{y}_d(t) = \hat{\Theta}(t)\,\Phi(t) \quad (8)$$

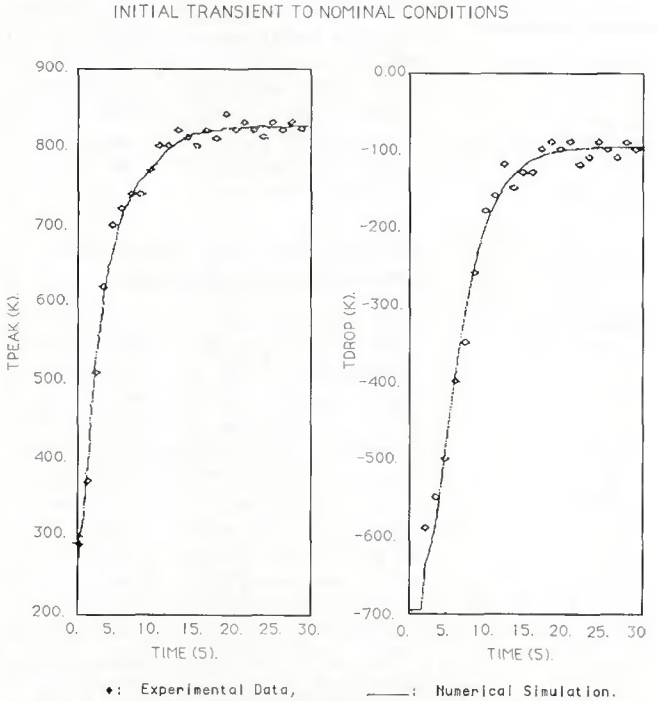

Fig. 11—Time responses of the welding outputs T_p and T_d during the transient to the nominal conditions ($Q_1^* = 2500$ W, $Q_2^* = 250$ W).

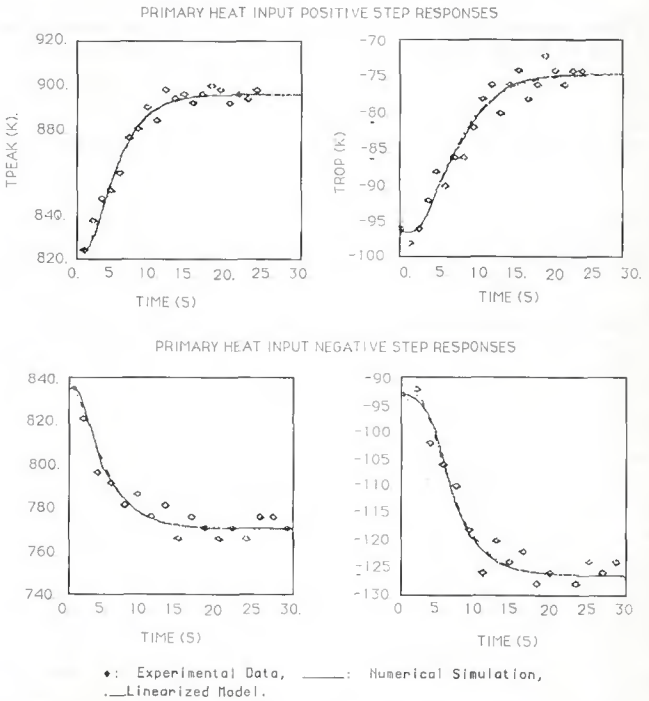

Fig. 12—Time responses of the welding outputs T_p and T_d during a positive and a negative step to Q_1 (from $Q_1^* = 2500$ W to $1.2\,Q_1^* = 3000$ W or $0.8\,Q_1^* = 2000$ W).

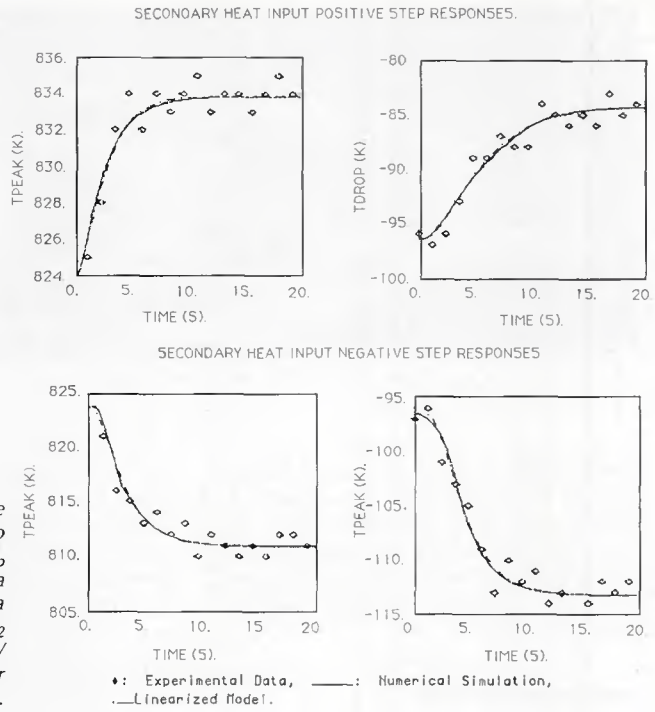

Fig. 13—Time responses to welding outputs T_p and T_d during a positive and a negative step to Q_2 (from $Q_2^* = 250$ W to $2Q_2^* = 500$ W or $0Q_2^* = 0.0$ W).

Moreover, this algorithm is modified by constraining the welding inputs Q_1 and Q_2 to feasible ranges, in-process modulation of the adaptation gain $\gamma(t)$ to insure solvability of the control law, and adding an external secondary control loop to improve the closed-loop performance (Ref. 21).

The experimental implementation of the closed-loop thermal control system is illustrated in Figs. 14 and 15, where the arrangement and configuration of the thermal sensor and process actuator are as in the modeling experiments. The nominal welding conditions used were identical to those described earlier under model calibration. The microcomputer (AT&T PC6300) executes the controller software (the above algorithm) with externally calibrated initial estimates of the 12 parameters in $\hat{\Theta}(0)$. The sampling period $T = 2T_t = 2.4$ s, which is the smallest integer number of welding gun cycles (for synchronous operation) that also satisfies the conditions for algorithm stability and is practically implementable, since it covers the process delays, thermal measurement, algorithm computation and actuator reaction times.

After the nominal conditions are reached, the closed-loop operation starts. Then, either a new reference command or a process disturbance is encountered and the resulting transient response is recorded. Each sampling period begins when a synchronization signal is transmitted from the actuator to the controller, at which time the welding robot starts the first gun cycle. After waiting for some time to compensate for the process delays, the computer sets the IR camera to the measurement mode. The infrared pyrometer senses the welding temperature field and transmits back to the computer the thermal profiles, first of the T_p sideline and then of the centerline. The camera is then reset to the monitoring mode, *i.e.*, the recording of thermal images for off-line processing, for the remaining part of the sampling period.

Next, the welding outputs T_p and T_d are evaluated in-process from the two line scan thermal profiles, and the control algorithm determines the necessary welding inputs Q_1 and Q_2 for their regulation to setpoints T_p^d and T_d^d. Thus, the actuator variables (the sectional velocities v_1, v_2 and the arc power Q) can be computed according to Equation 3, and transmitted as an actuator command to the welding robot through a second serial communication line. Finally, the computer saves the current sampling period results and waits for a new synchronization signal, at which time the robot has completed the second welding gun cycle and adjusts to the new values of the actuator variables for the next sampling period. This routine is repeated until the full test weld bead length (300 mm) is deposited.

Table 1—Transfer Function Parameters of the Linearized Model α[(a)]

Input	Output	Tpeak at Wp = 10.5 mm Tp (K)				Tdrop at T = 2.4 s Td (K)			
I	Step	K (K/W)	d (s)	w (rad/s)	T_{eq} (s)	K (K/W)	d (s)	w (rad/s)	T_{eq} (s)
Q_1 (W)	$+0.2Q_1^*$	0.144	1.0	0.410	4.38	0.0441	1.4	0.313	6.39
	$-0.2Q_1^*$	0.150	1.2	0.352	5.68	0.0546	1.7	0.321	6.24
	$+Q_2^*$	0.0394	0.	0.665	3.01	0.0489	0.2	0.357	5.60
	$-Q_2^*$	0.0522	0.	0.625	3.20	0.0671	0.6	0.476	4.20

(a) α = standard.

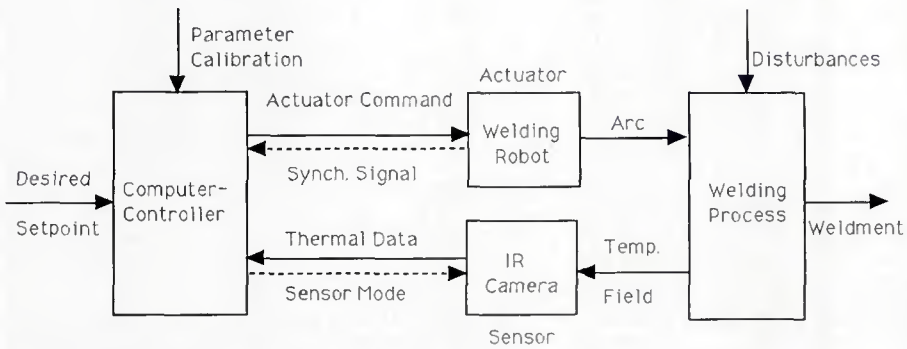

Fig. 14—Control equipment communication diagram.

Thermal Controller Performance Simulation and Experiment

The performance of the closed-loop system was tested using both simulation and experiments. The welding output and input responses of the thermal control system to a substantial simultaneous step in both the T_p and T_d setpoints are shown in Fig. 16. Also shown is the respective transients computed using the numerical simulation as the process model. While the general correspondence between simulation and experiment is quite good, variations among the transient responses and the steady-state deviations of welding inputs do occur because of modeling imperfections (parameter errors, unmodeled dynamics and nonlinearities). The desired welding outputs are tracked exactly at the steady state, and the transients

are smooth because of the mild input modulation, although the settling length is about 70 mm (2.8 in.).

Changes in desired heat-affected zone and cooling-rate conditions (and hence the setpoints for T_p and T_d) will be uncommon, and it is more likely that the control system will be required to maintain fixed setpoints so as to reject process disturbances, such as thickness changes, heat sink variations and arc changes. Accordingly, the performance of the thermal control system in maintaining the specified nominal conditions in the presence of unexpected process disturbances was first tested during a severe step change of the plate thickness (on the bottom plate surface) at t = 0, from 3.17 to 2 mm (0.125 to 0.08 in.). The experimental welding output and input responses are illustrated in Fig. 17, together with the computed transients with the numerical simulation (solid line) as the process model. The disturbance is eventually rejected at the steady state, with limited output deviations during the transient. Note, however, that the settling time (and equivalent settling length of 120 mm) is quite long, owing to the rather slow response of the system.

The disturbance rejection performance was also tested experimentally for other step disturbances. Figure 18 shows the effect of changes encountered at t = 0 in the material properties (mainly the thermal diffusivity and emissivity, which were induced by having the welding gun cross the boundary between plates of similar

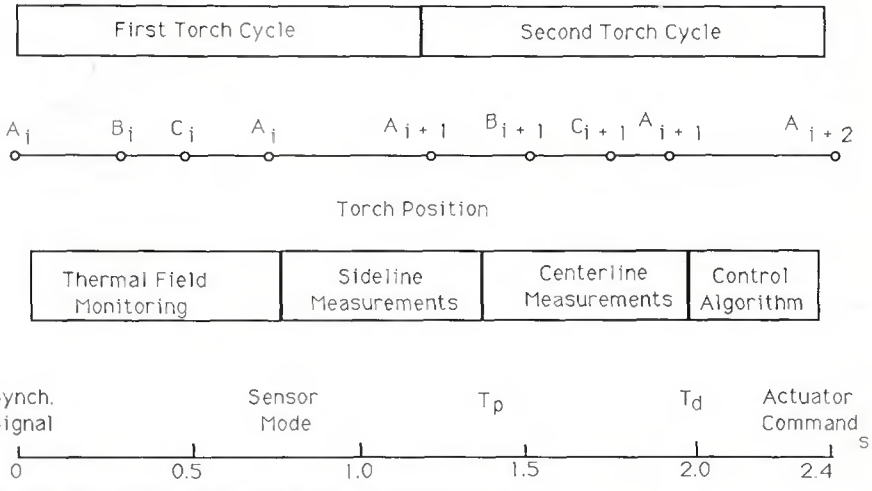

Fig. 15 — Actuator and controller synchronization diagram.

geometry but different steel), a temperature field (preheat) disturbance (implemented by driving the torch into another insulated plate, preheated by previous welding) and a disturbance in the process conditions (obtained by a step decrease of the average gun velocity to v = 9.5 in./s — 241 m/s). The figure shows that all disturbances are eventually rejected, although with a small steady-state deviation in the case of the material disturbance, since the undetectable change in the surface emissivity deceives the temperature measurements by the infrared radiation pyrometer. There are initial temperature field distortion effects at the boundary of separate plates (in the material and preheat case), and the steady-state input values after the velocity and preheat disturbance, given the stronger effect of Q_2 on T_d, indicate the preferential effect of preheat on cooling rate.

Simulation of an Enhanced System

While the controller performance is excellent with respect to the steady state, the settling time after the disturbances is quite long. To explore the effect of a faster and more decoupled control system, a modified model was developed, and a controller was designed assuming a faster measurement device and torch actuator. To reduce delays associated with

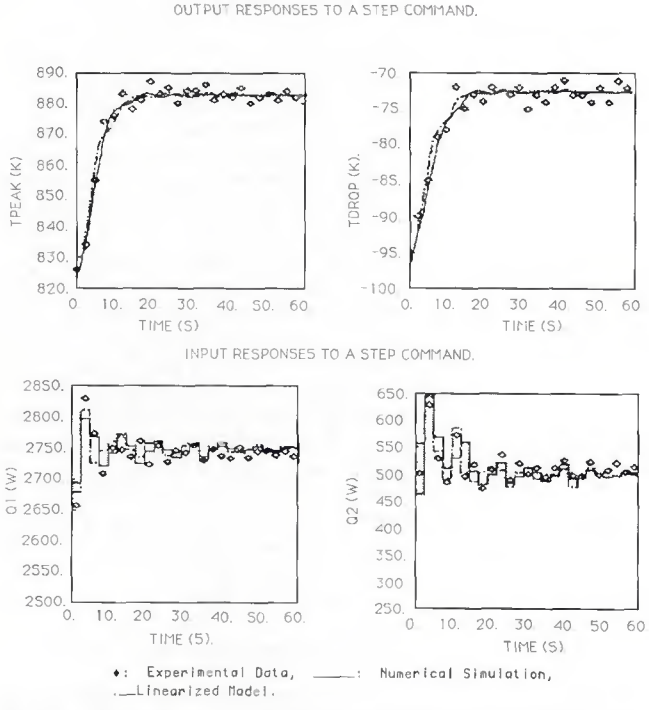

Fig. 16 — Time responses of the welding outputs and inputs after a step reference command (simplified 2 × 2 system).

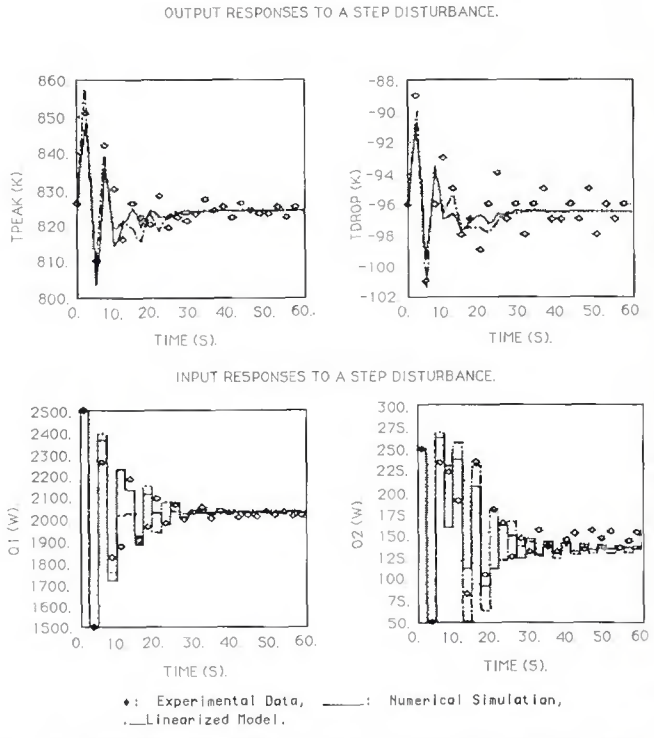

Fig. 17 — Time responses of the welding outputs and inputs after a step thickness disturbance (simplified 2 × 2 system).

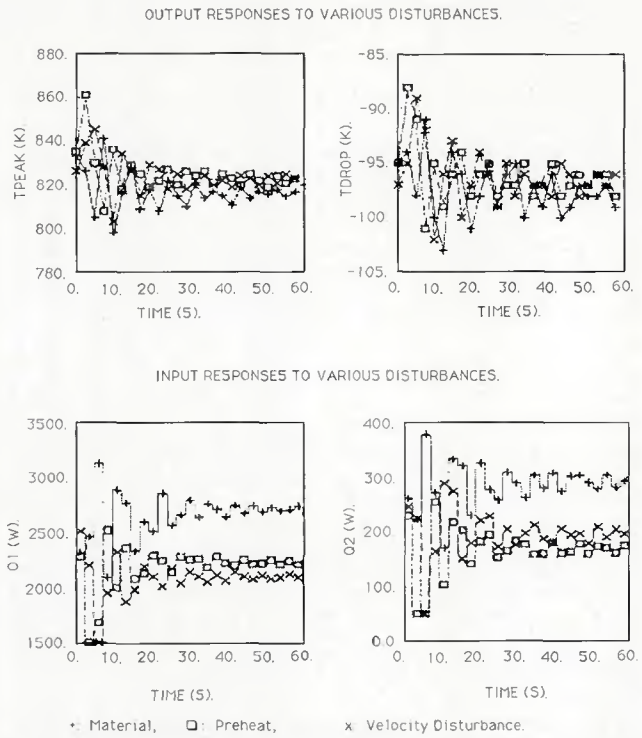

Fig. 18 – Time responses of the welding outputs and inputs after various step disturbances (simplified 2 X 2 system).

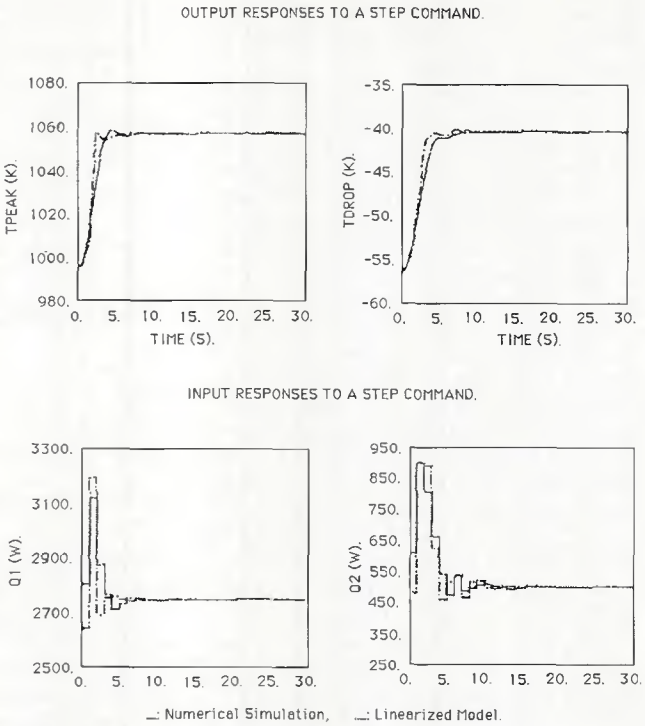

Fig. 19 – Time responses of the welding outputs and inputs after a step reference command (modified 2 X 2 system).

heat diffusion to the sideline, the welding output T_p' can be measured on a sideline at shorter distance $w_p' = 6.8$ mm (0.28 in.) from the centerline (*e.g.*, corresponding to the austenitization rather than recrystallization zone). With more rapid sampling, T_d' can be redefined relative to a shorter sampling period $T' = 1$s. Again, a set of first order equations (per Equation 6) were fit to simulated responses, based on the operations point

$Q_1^* = 2500$ W $\quad T_p^* = 996$ K
$Q_2^* = 250$ W corresponding to:
$T_d^* = -56.4$ K

The corresponding dynamics parameters are collected in Table 2. Compared with the parameters in Table 1, it is evident that T_p' is nearly decoupled from Q_2 and that the enhanced system is faster since the measurement locations of the welding outputs T_p' and T_d' are closer to the heat source.

The closed-loop performance of this modified process model, combined with a modified controller design, is compared to its open-loop behavior (*i.e.*, without a feedback controller) by simulation in Fig 19. The command following responses of the welding outputs and inputs after a step reference command, increasing the nominal values (T_p^*, T_d^*) by 60 K and 16 K, respectively, are shown in the figure. The closed-loop transients (using the numerical simulation as the process model).

The disturbance rejection regulation behavior is tested using the same step reduction in thickness as before, and is plotted in Fig. 20. The disturbance is rejected after a short settling time in both the closed-loop responses, in contrast to the open-loop behavior, in which the lack of feedback results in a large steady-state deviation from the nominal conditions.

In these references and disturbance rejection tests, the superior time domain performance arises from the speed and decoupledness of the modified process model, enabling the use of a simpler parametrization (8-parameter $\underline{\theta}'$) and shorter sampling period $T' = 1$ s used by the modified controller.

Fig. 20 – Time responses of the welding outputs and inputs after a step thickness disturbance (modified system).

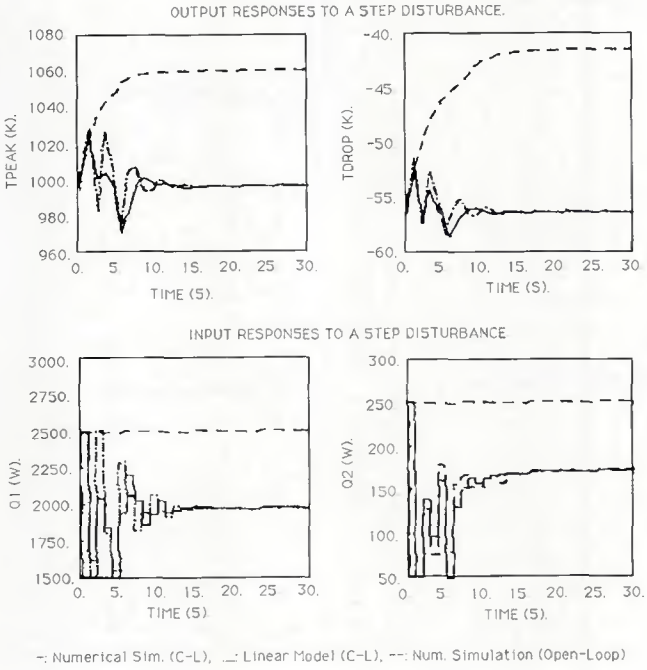

Range of Controllability

When developing an automatic control system, it is imperative to be concerned with the control authority or range of

achievable outputs that the inputs afford. For the case considered here, the ranges of achievable welding output values of the thermal control system for feasible ranges of the inputs Q_1 and Q_2 were determined approximately by numerical simulation, calibrated at the nominal conditions, and are depicted in Fig. 21. The line represents values of T_p and T_d for constant inputs magnitudes. The feasible reference setpoints for T_p and T_d are inside the enveloping line, and clearly there is more control authority in the lower heat input region. Although the input-output dependencies are coupled, the angles between the two curve families indicate the preferential effect of Q_1 on T_p or HZ, and of Q_2 on T_d or CR, and their spacing reflects their nonlinearity, especially of Q_2, as expected from the gain K values and variations in Table 2. At the high total arc power region, there is little further flattening of the local temperature hill slope at the critical centerline point x_d, as it shifts backwards, and thus little change of T_d or CR, while at the low arc power end the two peaks of the temperature hill are widely separated, and HZ is eventually decoupled from Q_2.

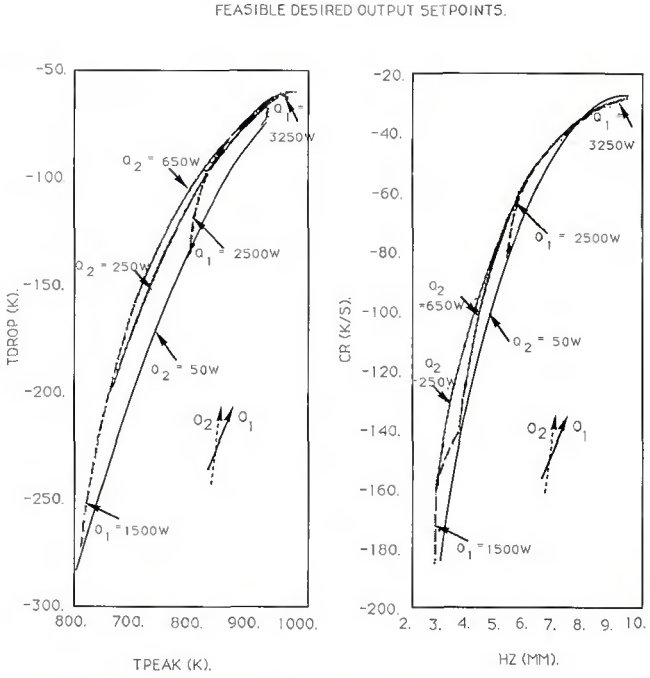

Fig. 21—Achievable steady-state setpoints of the welding outputs T_p, T_d and HZ, CR.

Table 2—Transfer Function Parameters of the Linearized Model β[(a)]

Input	Output	Tpeak at W'p = 10.5 mm T'p (K)				Tdrop at T' = 2.4 s T'd (K)			
I	Step	K (K/W)	d (s)	w (rad/s)	T_{eq} (s)	K (K/W)	d (s)	w (rad/s)	T_{eq} (s)
Q_1	$+0.2Q_1^*$	0.239	0.50	0.778	2.57	0.0340	0.96	0.439	4.55
(W)	$-0.2Q_1^*$	0.250	0.55	0.735	2.72	0.0439	1.06	0.493	4.05
	$+Q_2^*$	0.0008	0.	—	0.	0.0405	0.14	0.533	3.75
	$-Q_2^*$	0.028	0.	—	0.	0.0421	0.34	0.794	2.52

(a) β – standard.

Conclusions

In this paper, the concept of simultaneous regulation of both heat-affected zone and centerline cooling rate (CR) has been forwarded. The problem of regulating HZ and CR is transformed to one of controlling a peak temperature along a line parallel to the travel direction and the temperature drop over a fixed time interval along a line trailing the welding gun. The process modeling has revealed the inherent coupling in the welding dynamics, and a double gun system was proposed to achieve the necessary degree of control independence. An adaptive closed-loop system based on line-scan IR temperature measurement was designed and has demonstrated the ability to independently regulate T_p and T_d. More importantly, the system has shown the ability to reject the effect of typical process disturbances. It is this disturbance rejection that most clearly illustrates the simultaneous output regulation properties of this system.

It must be observed that the translation of the problem from one of regulating specific metallurgical boundaries and states to one of regulating surface temperature histories, requires that the metallurgical processes involved in a particular welding situation be understood *a priori*. However, given that specific reference setpoints for T_p and T_d could be specified by such prior knowledge, the work presented here demonstrates clearly the ability to independently regulate these two thermal quantities, albeit within the limited range of control authority afforded by the process.

At this time, the primary performance limitations in the process are measurement and actuator speed. These place an upper limit on the response time of the control system to either command changes or external disturbances. This observation was confirmed by simulating a hypothetical "enhanced" system, where different measurements and measurement systems led to greatly improved response time. Definition of the welding outputs close to the heat source is essential for the process model speed, while decoupledness is additionally favored by small thermal diffusivity and long secondary welding gun distance x. The welding input modulation range, limited to avoid catastrophic melt-through or excessive porosity and incomplete fusion, should be maximized by proper experimental selection of the nominal conditions. This is also essential to avoid the GMAW process noise, stemming from arc instabilities and the globular metal transfer mode.

The thermal sensor used here is primarily responsible for the long sampling period T, and thus, the speed limitations of the experimental closed-loop system. Also, the temperature resolution of the infrared pyrometer and the resulting quantization may inhibit fine regulation of the welding outputs, and the spatial camera resolution poses an upper bound to the monitored length of the weld bead. Finally, the effects of in-process emissivity variations, as already discussed, are inevitable as long as radiation measurements are performed at a single wavelength range, necessitating emittance independent infrared analysis (EIIA) techniques.

The use of the time multiplexed torch system is an effective means for distributing the heat input. However, as mentioned above, it may produce an undesirable bead geometry. In this case, a secondary trailing torch (most likely GTA) could be used, at the cost of a second power supply and potential electrical interaction with the primary arc.

To the authors' knowledge, this research represents the first demonstration of simultaneous regulation of the primary thermal characteristics of a weld. The impact of closed loop control of these quantities is clear and dramatic, and if

properly developed and exploited could lead to more carefully, and less conservatively designed joints, particularly for heat-sensitive alloys. Thus, it may contribute to the optimization of welding productivity and further may permit previously unweldable materials to be successfully joined. Future research at MIT will focus on refinement of the experimental apparatus to improve response speed, and to exploration of a wider range of welding conditions. Finally, it is hoped that this thermal control system can be welded to a corresponding weld profile controller (described in Ref. 30) to yield simultaneous geometry and thermal history control, thereby approaching the goal of the integrated welding process control system.

Acknowledgments

This work was supported by the U.S. Dept. of Energy under Contact No. DE-FG02-85ER13331. The authors gratefully acknowledge the help of Dr. Michael Hale in reviewing this manuscript, and Prof. Thomas Eagar for advice and for providing the IR sensing equipment for the experiments.

References

1. Richardson, R.W., Gutow, D. A., and Rao, S. H. 1982. A vision-based system for weld pool size control. *Measurement and Control for Batch Manufacturing,* ed. Hardt, pp. 65-67.

2. Hardt, D. E., Garlow, D. A., and Weinert, J. B. 1985. A model of full-penetration arc welding for control system design. *Trans. ASME, Journal of Dynamic Systems, Measurement and Control,* Vol. 107.

3. Linnert, G. E., *et al.* 1968. *Arc Welding,* Metals Engineering Institute, ASM.

4. Udin, H., Funk, and E. R., Wulff, J. 1967. *Welding for Engineers,* J. Wiley & Sons, N.Y.

5. Masubuchi, K. 1980. *Analysis of Design and Fabrication of Welded Structures.* Pergamon Press, N.Y.

6. McClintock, F. A., and Argon, A. S. 1966. *Mechanical Behavior of Materials,* Addison-Wesley.

7. Doumanidis, C. 1986. A survey of the effects of weld imperfections on the fracture toughness of the joint. Unpubl. Report 2.301, M.I.T.

8. Doumanidis, C. 1986. Real-Time Control of Thermal Properties in Welding. LMP research report LMP/FAR 86-05, M.I.T.

9. Doumanidis, C. 1988. Modelling and control of thermal phenomena in welding. Ph.D. Thesis, Department of Mechanical Engineering, M.I.T.

10. Rosenthal, D. 1941. Mathematical theory of heat distribution during welding and cutting. *Welding Journal* 20(5):220-s to 234-s.

11. Carslaw, H. S., and Jaeger, J. C. 1959. *Conduction of Heat in Solids.* 2nd Edition, Oxford Press, London U.K.

12. Myers, P. S., Uyehara, O. A., and Borman, G. L. 1967. Fundamentals of heat flow in welding. *Weld. Res. Council Bulletin* 123.

13. Mahla, E. M., Rowland, M. C., Shook, C. A., and Doan, G. E. 1941. Heat flow in arc welding. *Welding Journal* 20(7):459-468.

14. Jackson, C. E., and Shrubsall, A. E. 1953. Control of penetration and melting ratio with welding technique. *Welding Journal* 32(2):172-s to 178-s.

15. Cristensen, N., Davies, V. L., and Gjermundsen, K. 1965. The distributions of temperatures in arc welding. *Brit. Weld. J.* 12:54-75.

16. Nippes, E. F., and Savage, W. F. 1949. Development of specimen simulating weld heat-affected zones. *Welding Journal* 28(6): 534-s to 546-s.

17. Alberry, P. J., and Jones, W. K. C. 1982. Computer model for prediction of HAZ microstructures in multipass weldments. *Metals Tech.* 9:419-426.

18. Hibbitt, H. D., and Marcal, P. V., 1973. A numerical thermomechanical model for the welding and subsequent loading of a fabricated structure. *Computers and Structures* 3(5):1145-1174.

19. Doumanidis, C. 1986. A numerical simulation of the welding process. LMP Research Report LMP/FAR 86-06, M.I.T.

20. Doumanidis, and C, Hardt, D. 1989. A model for in-process control of thermal properties during welding. *ASME Journal of Dynamic Systems, Measurement and Control,* 22, No. 2.

21. Doumanidis, and C., Hardt, D. 1990. Multivariable adaptive control of thermal properties in welding. To be published in the *ASME Journal of Dynamic Systems, Measurement and Control.*

22. Giedt, W. H., Wei, X. C., and Wei, C. R. 1984. Effect of surface convection on stationary GTA welding zone temperatures. *Welding Journal* 63(12):376-s to 383-s.

23. Chin, B. A., Madsen, N. H., and Goodling, J. S. 1983. Infrared thermography for sensing the arc welding processes. *Welding Journal* 62(9): 227-s to 234-s.

24. Boillot, J. P., Cielo, P., Begin, G., Michel, C., Lessard, M., Fafard, P., and Villemure, D. Adaptive welding by fiber optic thermographic sensing: an analysis of thermal and instrumental considerations. *Welding Journal* 64(7):209-s to 217-s.

25. Warmeatlas. 1974. *Berechnungsblatter fur den Warmeubergang,* VDI Verlag, Dusseldorf, West Germany.

26. Inframetrics, Inc. 1985. *Installation and Operation of the Inframetrics Model 600IR Imaging Radiometer.* 4625 Rev. B, Bedford, Mass.

27. Thermoteknix Systems Ltd. 1986. *Operating Instructions for the Thermagram Thermal Image Processing System.* Cambridge U.K.

28. Goodwin, G. C., Ramadge, P. J., and Caines, P. E. 1980. Discrete-time multivariable adaptive control. *IEEE Trans. on Aut. Control,* Vol. AC-25 No. 3, pp. 449-456.

29. Doumanidis, C. C., Hale, M., and Hardt, D. E. 1986. Multivariable control of arc welding processes. *Advances in Welding Science and Technology,* ASM International, Materials Park, Ohio.

30. Hale, M. B. 1989. Multivariable dynamics modeling and control of GMAW weld pool geometry. Ph.D. Thesis, M.I.T.